Pharm Res (2017) 34:2066–2074
DOI 10.1007/s11095-017-2211-6

RESEARCH PAPER

Computational Analysis on Down-Regulated Images of Macrophage Scavenger Receptor

Byeongtaek Oh[1,2] • Yugyung Lee[3] • Mingui Fu[4] • Chi H. Lee[1]

Received: 10 May 2017 / Accepted: 13 June 2017 / Published online: 26 June 2017

ABSTRACT

Background Thiolated-graphene quantum dots (SH-GQDs) were developed and assessed for an efficient preventive means against atherosclerosis and potential toxicity through computational image analysis and animal model studies.

Experiments Zebrafish (wild-type, wt) were used for evaluation of toxicity through the assessment of embryonic mortality, malformation and ROS generation. The amounts of SH-GQDs uptaken by mouse macrophage cells (Raw264.7) were analyzed using a flow cytometer. For the time-dependent cellular uptake study, Raw264.7 cells were treated with SH-GQDs (200 μg/ml) at specific time intervals (0.5, 1, 2, 5, 10 and 24 h). The efficacy of SH-GQDs on DiO-oxLDL efflux by Raw264.7 cells was evaluated (DiO, 3,3′-dioctadecyloxacarbocyanine) based on the percentage of positive cells containing DiO-oxLDL. TEER of human primary umbilical vein endothelial cells (hUVECs) were examined to assess the barrier function of the cell layers upon being treated with oxLDL.

Results SH-GQDs significantly enhanced the efflux of oxLDL and down-regulated macrophage scavenger receptor (MSR) in Raw264.7. The ROS levels stimulated by oxidative stress were alleviated by SH-GQDs. oxLDL (10 μg/ml) significantly impaired the barrier function (TEER) of adherence junctions, which was recovered by SH-GQDs (10 μg/ml) (oxLDL: 67.2 ± 2.2 Ω-cm^2 for 24 h; SH-GQDs: 114.6 ± 8.5 Ω-cm^2 for 24 h). The mortality rate (46% for 1 mg/ml) of the zebra fish increased, as the concentrations and exposure duration of SH-GQDs increased. SH-GQDs exerted negligible side effects.

Conclusion SH-GQDs have target specificity to macrophage scavenger receptor (MSR) and efficiently recovered the ROS levels and TEER. SH-GQDs did not induce endothelial cell layer disruption nor affected zebrafish larvae survival.

KEY WORDS macrophage scavenger receptor (MSR) · oxLDL · theranostic carrier · thiolated-graphene quantum dots (SH-GQDs)

ABBREVIATIONS

ABCA1	ATP-binding cassette transporter
DCFDA	Dichlorofluorescin diacetate
MSR	Macrophage scavenger receptor
oxLDL	oxidized-low density lipoprotein
ROS	Reactive oxygen species
SH-GQDs	Thiolated-graphene quantum dots
TEER	Trans-epithelial Electrical Resistance

INTRODUCTION

Inflammatory milieu of atherosclerosis interactively evolves with various molecular imaging devices and advanced nanotechnology. Atherosclerotic plaque rupture is usually followed by a rapid or delayed type of occlusive thrombus formation, causing acute ischemic stroke. There is an urgent need for new clinical tools to efficiently alleviate the formation of atherosclerotic plaque (1). Optical molecular imaging has emerged as a new means that can specifically label extra- and intra-cellular

✉ Chi H. Lee
leech@umkc.edu

[1] Division of Pharmaceutical Sciences, School of Pharmacy, University of Missouri-Kansas City, 2464 Charlotte Street, HSB-4242, Kansas City, Missouri 64108, USA

[2] Present address: Department of Neurology and Neurological Sciences, School of Medicine, Stanford University, Stanford, California 94305, USA

[3] School of Computing and Engineering, University of Missouri-Kansas City, Kansas City, Missouri 64108, USA

[4] Department of Biomedical Science and Shock/Trauma Research Center, School of Medicine, University of Missouri-Kansas City, Kansas City, Missouri 64108, USA

biomarkers of cardiovascular diseases, accomplishing real-time monitoring of disease progress with high spatial resolution to image-specific molecular targeting (2).

The successful application of image-guided theranostic agents to the cardiovascular diseases requires that drugs or a carrier as a whole should be imaged locally or activated at the targeted site via functional nanomaterials (3). The most critical features of an efficient theranostic agent that may serve as a major challenge in the FDA approval process are; a) a proper analysis tool for the accurate image assessment of the molecular pathogenesis at the systems level, b) a smart design that allows for a nano-agent to sensitively regulate its theranostic function in response to the progressive pathologic milieu *in vivo* and customize to individual subjects, and c) they should be free of side effects even after their long resident time in the body (4–6).

As of now, numerous noninvasive image-guided modalities, such as autoradiography magnetic resonance imaging (MRI), ultrasound (US), optical imaging, X-ray computed tomography (CT), positron emission tomography (PET), single-photon emission computed tomography (SPECT), electron microscopy, and autoradiography, have been used to provide images not only at a tissue level but also at the molecular level in biomedical and clinic settings (7). Among them, PET and optical imaging techniques are considered as quantitative imaging modalities, whereas CT and MRI are normally used for anatomical imaging analysis (8,9). Fluorescence resonance energy transfer (FRET) microscopy has been considered as a sensitive and reliable biological device for diagnosis of conclusive cardiovascular disease (10). The efficiency and biocompatibility of donor–acceptor pairs are fundamental to improve the accuracy of fluorescence resonance energy transfer and the subsequent analytical performance (11). However, fluorescent probes including organic dyes and inorganic semiconductor quantum dots (QDs) have their own drawbacks, such as poor photo-stability, liable to photo-bleaching, small stokes shifts and short half-life shown by most organic dyes (12,13).

Although the popular pharmacologic tools including nanomedicines (NMs) have been widely used to systemically alleviate conclusive cardiovascular disease, various side effects as well as the lack of therapeutic efficacy and diagnostic property have posed as a main obstacle for their clinical application. Graphene nanoparticles were effective in reducing lipopolysaccharide-induced nitric oxide production through the inhibition of NF-κB and IFN-β/STAT1 pathways in RAW264.7 macrophage cells (14). Thiolated-graphene quantum dots (SH-GQDs) developed using hydrothermal pyrolysis technique from our laboratory were characterized for their sizes and quantum yields, and have shown their excellent efficiency in alleviation of the atherosclerosis progress (15). SH-GQDs are capable of performing targeted delivery via universal ligand–receptor recognition in nature, and displaying superb biocompatibility at the cellular level from the studies on bio-distribution and cell apoptosis analysis. It was also found that SH-GQDs stimulated the efflux of oxLDL (oxidized-low density lipoprotein) through over-expressed ABCA1 and scavenge ROS in inflamed macrophages (15).

The pathological process responded by macrophages is their failure to handle modified lipoproteins, leading to foamy cell formation that is an essential ingredient of atherosclerotic plaques. Macrophage scavenger receptors (MSR) is the integral molecules responsible for the recognition and administering of modified lipoproteins. Certain MSRs could exert resilient reactions, whereas some MSRs react to modified lipoproteins by accumulation and augmentation of inflammation factors in the plaque (16). The enhancement of lipid efflux and down-regulation of MSR in mouse macrophage cell line (Raw264.7) by SH-GQDs would support its promising usage as a theranostic carrier to prevent foam cell formation and subsequently monitor the progress of atherosclerotic plaque. The relationship among the expression levels of macrophage scavenger receptor A (MSR-A), lipid accumulation and ROS production in macrophages could be established to optimize SH-GQDs as an efficient preventive means against atherosclerosis.

The assessment of the treatment processes of up-normal blood pressure and cardiovascular diseases mediated through multi-functional nanomaterials has been relied on various molecular images from the small animal models and cutting-edge biotechnology. Zebrafish has been used as a prognostic model for the assessment of potential toxicity of nanomaterials in cardiac development. Zebrafish shares a high degree of functional and sequential homology with humans and, therefore, studies in Zebrafish have provided with great insight into human disease processes. The evolving embryos in zebrafish are reasonably sensitive to nanomaterials and the heart is formed as a first organ during the development process of transparent embryos (17,18). Zebrafish has blood cell types similar to human beings (19,20).

Zebrafish embryos and larvae having wholly transparent nature can assess the impact of a pharmacological treatment or genetic manipulation via non-invasive imaging techniques that caused less animal suffering and avoided any influences of experimental conditions on the experimental outcome. Thus, the zebrafish model allows for thorough investigation on more prominent development of vascular infection by numerous inducers and is suitable for large-scale genetic and high-throughput screening of mechanism and endpoints of toxicity involved with cardiovascular diseases (21).

In this study, we determined the amounts of SH-GQDs uptaken by Raw264.7 cells and DiO-oxLDL efflux, and established the relationship among the expression of macrophage scavenger receptor A (MSR-A), lipid accumulation and ROS production in macrophages. We also evaluated the barrier functions of cell layers upon exposure to SH-GQDs via quantification of Trans-epithelial Electrical Resistance (TEER). As a critical step towards the clinical translation,

the optimized SH-GQD with the most effective outcomes was chosen as the theranostic carrier, and the toxicity assessment was performed in the zebrafish models via computational image analysis of embryonic mortality, malformation and ROS generation.

METHODS AND MATERIALS

Materials

Reduced-glutathione (GSH), citric acid, phosphoric acid, lipopolysaccharides (LPS), sulfanilamide, dichlorofluorescein diacetate (DCFDA), N-1-napthylethylenediamine dihydrochloride, dextran sulfate, sodium azide and dextran sulfate were purchased from Sigma-Aldrich (St. Louis, MO).

Mouse macrophage cell line (Raw264.7), Dulbecco's modified eagle's medium (DMEM) (30–2601) and penicillin-streptomycin solution (30–2300) were purchased from ATCC (Manassas, VA). Fetal bovine serum (FBS) was purchased from Atlantic biological (Atlanta, GA). All other reagents and solvents were of analytical grade.

Preparation of Thiolated-Graphene Quantum Dots (SH-GQDs)

SH-GQDs were prepared using thermal treatment of carbon source (citric acid) in the presence of a surface modifier (reduced-glutathione, GSH). Briefly, citric acid (20% (*w*/*v*)) and GSH (20% (*w*/*v*)) were dissolved in deionized (DI) water (15). Briefly, 250 µl of solution was transferred into pre-heated glass vial placed in the oil bath (equilibrated at 150°C) (OD = 1.3 cm, Screw thread with rubber lined cap, Fisher, Pittsburgh, PA), and then vial was thermally treated for 15 min. After the hydrothermal process, the black thick film layer was reconstituted with H_2O, and pH was adjusted to 7.4 using 1 M of NaOH. The solution was further dialyzed using a dialysis bag (3500 MWCO, BioDesign, Carmel, NY) (Size: approximately 20 nm; Quantum yields (QYs): 0.55) to remove unreacted citric acid and GSH. GQDs were prepared using the same method as used for SH-GQDs except the absence of GSH in the citric acid solution.

In vitro Cellular Uptake Study

Raw264.7 cells (3×10^5/well in 500 µl) were seeded on a 24-well plate and incubated for overnight. Cells were treated with varying concentrations of SH-GQDs (10, 20, 50, 100 and 200 µg/ml) at 37°C for 24 h. After the incubation process, cells were gently washed with the cold PBS solution three times to remove SH-GQDs remained on the surface of cells. After washing cells with PBS, cells were scraped and centrifuged to collect the cell pellet. The cells were suspended again in flow cytometry buffer containing 1% (*w*/*v*) BSA and 0.1% sodium azide. The amounts of SH-GQDs uptaken by cells were analyzed using a BD FACSCanto II flow cytometer equipped with BD FACSDiva software (BD Biosciences, San Jose, CA). For the time-dependent cellular uptake study, cells were treated with 200 µg/ml of SH-GQDs at specific time intervals (0.5, 1, 2, 5, 10 and 24 h). After the treatment, the cells were collected and analyzed using the same method as previously described.

For further elucidation of the cellular uptake mechanism and a pathway for SH-GQDs on Raw264.7 cells, cells were incubated with various conditions, such as low temperatures (4°C), ATP-depleted condition and pre-treatment with dextran sulfate (10 µg/ml) in the presence of SH-GQDs (50 µg/ml). For ATP-depleted condition, the cells were pre-treated with 50 mM 2-deoxy-$_D$-glucose and 25 mM NaN_3 for 1 h.

Effects of SH-GQDs on oxLDL Efflux

The efficacy of SH-GQDs on DiO-oxLDL efflux (human DiO-medium oxidized LDL (DiO, 3,3′-dioctadecyloxacarbocyanine, ex: 485 nm; em: 515 nm) (Kalen Biomedical, LLC, Montgomery Village, MD) by Raw264.7 cells was evaluated based on the percentage of positive cells containing DiO-oxLDL. In brief, cells were treated with DiO-oxLDL in DMEM (2 µg/ml) for 24 h. After the incubation, cells were treated with the media (the positive control) and SH-GQDs (50 µg/ml). Cells were collected and resuspended in the flow cytometry buffer, and DiO mean fluorescence intensity of intact single cells were quantitated. The obtained data expressed in the mean fluorescence intensity were background subtracted and the amount of oxLDL uptake was normalized as the percentage oxLDL uptake of the DMEM treatment (i.e. the positive).

Assessment of Transepithelial Electrical Resistance (TEER) of Cell Layers

TEER was examined to assess the barrier function of cell layers upon being treated with various environmental conditions. To evaluate TEER of human primary umbilical vein endothelial cells (hUVECs) against oxLDL, hUVECs (PCS-100-010), vascular cell basal medium (PCS-100-030) and endothelial growth kit–VEGF (VEGF, vascular endothelial growth factor) (PCS-100-041) purchased from ATCC (Manassas, VA) were used. The medium was gently mixed with growth supplements and kept in the refrigerator at 4°C. hUVECs were cultured under the standard cell culture conditions (5% CO_2 and humidified air at 37°C).

As cells were confluent, hUVECs with 5×10^5 per well were seeded on the apical side of inserts (pore size = 3 µm and surface area = 1.12 cm^2) (Corning Costar Transwell,

Corning Incorporated, Tewksbury, MA) freshly coated with 50 μg/ml of human fibronectin in 12-well plate and cultured for 2 days. The cells were treated with oxLDL (10 μg/ml) in the presence of GQDs or SH-GQDs (10 μg/ml) and TEER values were measured using the epithelial volt-ohm meter (EVOM) and STX2 electrode (World Precision Instruments, Sarasota, FL). The final resistance after subtracting background TEER was presented as **Ω**-cm^2 (TEER × surface area).

Assessment of the Amount of Nitric Oxide (NO) Produced from hUVECs

Nitric Oxide (NO) produced from hUVECs upon cellular interaction with VEGF was quantified using the Griess assay (22). The Griess reagent was prepared by mixing of 0.1% N-(1-Naphthyl) ethylenediamine dihydrochloride (NED) dissolved in DI water and 1% sulfanilamide dissolved in 5% (*v*/v) phosphoric acid solution.

hUVECs with 2×10^4 per well were seeded on 96-well plate and cultured for overnight until cells were fully attached. The cells were treated with various treatment groups, such as media, L-NAME (1 mM), oxLDL (10 μg/ml) and oxLDL, in the presence of SH-GQDs (1, 5 and 10 μg/ml). After the incubation for 24 and 48 h, 100 μl media in the plate were transferred to fresh 96-well plate and 1% sulfanilamide solution (50 μl) was added to each well. The plate was incubated at room temperature for 5 min, and then, 0.1% NED solution (50 μl) was added to each well. The absorbance was measured at 550 nm using the multimode detector and extrapolated to the concentration of NO (μM).

Assessment of the ROS Accumulation Rates in the Zebrafish Model

Zebrafish was used as the animal model for evaluation of the ROS accumulation rates and toxicity. A total of 40 locally bred and reared short-fin wild type zebrafish from group housing tanks, initially on a recirculating AHAB system (Aquatic Ecosystems, Florida, USA), were used as subjects (23). Zebrafish (wild-type, wt) were raised in an environmentally controlled facility (Water: egg water (0.6 g/L sea salt); Photoperiod: 14 h light/10 h dark cycle; and Temperature: 28 ± 0.5°C). For such studies as embryonic mortality, malformation, and ROS generation assessment, fertilized eggs were collected and placed in 24-well plates (2 ml of 30% Danieau's solution (58 mM NaCl, 0.7 mM KCl, 0.4 mM $MgSO_4$, 0.6 mM $Ca(NO_3)_2$, 5 mM Hepes, pH 7.4) per well). Eggs were treated with varying concentrations of SH-GQDs (0.02, 0.05, 0.1, 0.2, 0.3, 0.6, 0.8, and 1 mg/ml) for 7 dpf (dpf: days-post fertilization). In all experiments, dead embryos and larvae were separated from the 24-well plates every 24 h.

The amount of ROS accumulated in zebrafish larvae was assessed for cytotoxicity study. First, larvae collected at 48 hpf (hours post-fertilization) were pretreated with SH-GQDs (25, 100, 200 and 300 μg/ml) along with ROS-sensitive dye (25 μM DCFDA) for 30 min. After the incubation, stained larvae were transferred to fresh media in 96-well plate, and then incubated with various treatment groups, such as media, hydrogen peroxide (H_2O_2, 50 μM) and H_2O_2 in the presence of SH-GQDs. The fluorescence level was measured using the multimode detector (DTX 880, Beckman Coulter Inc., CA) every 10 min (excitation 485 nm and emission 515 nm). The spontaneous fluorescence augmentation due to oxidation of DCFDA by ROS was recorded for the respective well without larvae. The H_2O_2 treatment group was served as a positive control.

Statistical Analysis

Data were presented as a mean ± standard deviation (S.D.). One-way ANOVA was used to compare the means of independent samples. F-ratio was determined using SPSS software (SPSS, Chicago, IL) and Tukey's HSD was used for a post-hoc analysis. *P*-values of less than 0.05 were considered as statistically significant. All experiments were conducted in triplicate unless otherwise specified**.**

RESULTS AND DISCUSSIONS

Assessment of the Uptake Rates of SH-GQDs by Macrophages

The cellular imaging analysis has provided crucial information in assessment of the efficacy of the endocytosis process. It was found that SH-GQDs with high quantum yields can be utilized to label single-cell biophysics in the absence of any extra fluorescent dyes. Thus, the suitability of SH-GQDs for theranostic application was assessed by elucidating the interaction of SH-GQDs with Raw264.7 and the uptake mechanism of SH-GQDs by Raw264.7.

To evaluate the uptake rate of SH-GQDs, the fluorescence values from cells treated with varying concentrations of SH-GQDs (10, 20, 50, 100 and 200 μg/ml) were examined using a flow cytometry. As shown in Fig. 1a, there was a dose-dependent increase in mean fluorescence intensity at the concentrations ranging from 10 to 200 μg/ml. Flow cytometry analysis was conducted to investigate the cellular uptake rates of SH-GQDs by Raw264.7. The macrophages were treated with varying concentrations of SH-GQDs. It was found from the histogram peaks of flow cytometry analysis (Fig. 1b) that the percentages of positive cells increased from 7.2 ± 0.1% to 49.1 ± 1.5%, as the concentration of SH-GQDs increased from 10 μg/ml to 200 μg/ml. To estimate the parameters of

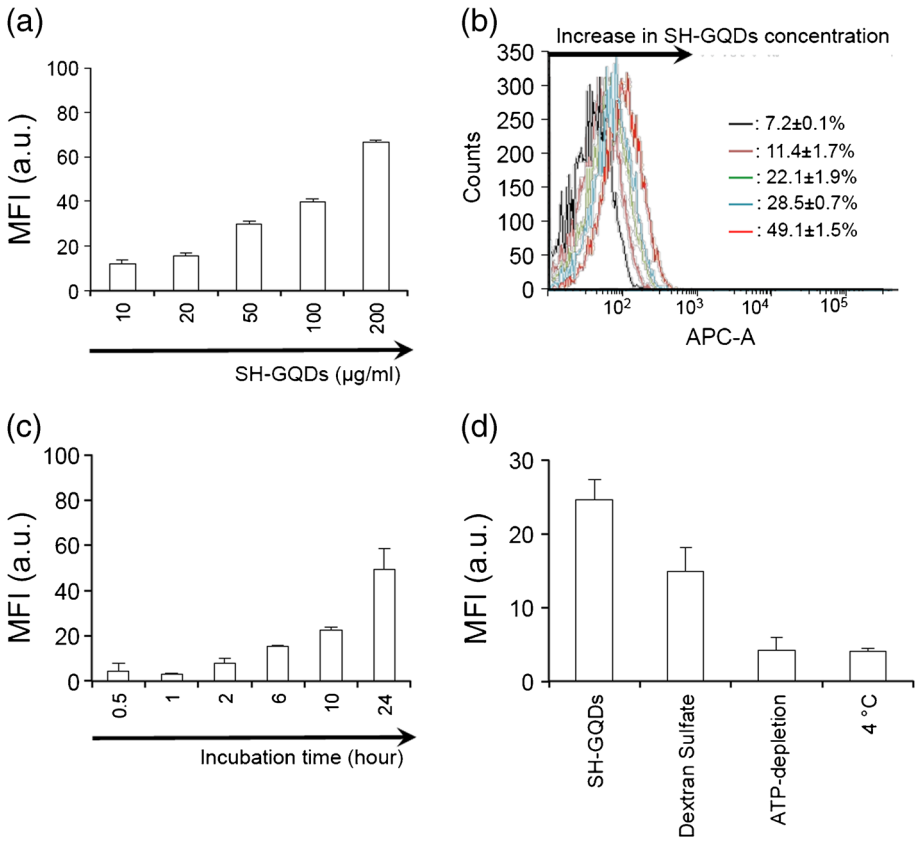

Fig. 1 (**a**) Flow cytometry cellular uptake assay of SH-GQDs ($n = 3$). Raw264.7 cells were incubated with varying concentration of SH-GQDs (10, 20, 50, 100 and 200 μg/ml) for 24 h at 37°C. (**b**) Flow cytometry histogram illustrating cellular uptake of SH-GQDs. Inset: Histogram showed a peak-shifted to right as SH-GQDs concentration increased (7.2 ± 0.1% to 49.1 ± 1.5%). (**c**) Flow cytometry cellular uptake assay of SH-GQDs (200 μg/ml) with varying incubation time (0.5, 1, 2, 5, 10 and 24 h) ($n = 3$). MFI indicates mean fluorescence intensity. (**d**) MFI for SH-GQDs (50 μg/ml) incubated in Raw264.7 cells for 24 h under different conditions, including negative (37°C), 4°C, dextran sulfate (scavenger receptor-A ligands) and ATP-depletion (50 mM 2-deoxy-$_D$-glucose and 25 mM NaN_3) ($n = 3$).

the uptake kinetics, macrophages were incubated with 200 μg/ml SH-GQDs for various time intervals (30 min, 1, 2, 6, 10 and 24 h) (Fig. 1c). The uptake rates of SH-GQDs followed a time-dependent profile. For up to 2 h after the incubation, there was no noticeable increase in intensity, whereas the significant amount of the SH-GQDs was cellular uptaken at10 hr. after the incubation, and afterward the uptake rate increased as a function of time (for 24 h, 49.4 ± 8.8).

It was a well-known fact that endocytosis is generally energy-dependent uptake process which can be slowed as the cells are incubated at low temperature (4°C) or under the ATP-depleted condition (24). The mean fluorescence intensity levels from the cells incubated at 4°C or under the ATP-depletion condition were lower than those from the medial control (Figw. 1d). Dextran sulfate, a nonspecific class A scavenge-receptor blocking agent, was tested to further investigate the uptake mechanism of SH-GQDs involved with MSR. When cells were pre-incubated with dextran sulfate (0.5 μg/ml), mean fluorescence intensity was lower than that of the control. In confocal microscopy image analysis, the fluorescent levels of the macrophages treated with SH-GQDs for 24 h were much greater than those of the untreated control (Fig. 2).

As biological images should have the proper brightness and contrast for easy viewing, the contrast control of a monitor was used to adjust the image intensities of the confocal microscopy images of Raw 264.7 cells upon being treated with SH-GQDs (200 μg/ml). The results are in a good agreement with previous reports that nanoparticles could be uptaken by macrophages via macrophage scavenge receptors (MSR and CD36). (25,26) As SH-GQDs may enter macrophage via some additional mechanisms other than MSR mediated process, dextran sulfate, that mainly shut down MSR mediated passage, only partially blocked the SH-GQDs uptake (Fig. 1d). These results supported that SH-GQDs could enter macrophages via MSR-mediated endocytosis mechanism that is an energy-dependent process.

Effects of SH-GQDs on oxLDL Efflux

Lipid-laden macrophages produce foam cells, gradually evolving into plaque at atherosclerotic lesion. Thus, the mechanism behind atherogenesis has largely focused on the role of interactions between lipoprotein and macrophages in the foam cell (27) and the enhancement of lipid efflux is considered as an ideal approach to mitigate the plaque progression. The efflux of oxLDL from macrophages was promoted by pretreatment of cells with DiO-oxLDL. As shown in Fig. 3, the study on the efflux of oxLDL from macrophages revealed that the oxLDL efflux was significantly enhanced in the cells treated with SH-GQDs for 24 h as compared to that treated with the media control (SH-GQDs: 39.2 ± 2.2%).

There was a significant difference in the efflux amount of oxLDL incubated with SH-GQDs between two treatment periods (3 h: 73.9 ± 1.5% and 24 h: 39.2 ± 2.2%), indicating

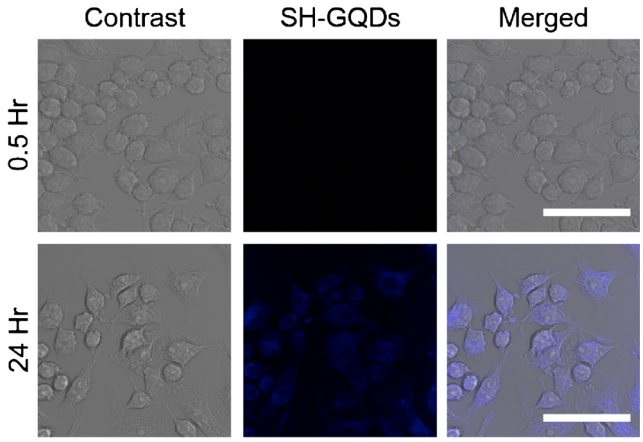

Fig. 2 Bright field images and corresponding confocal microscopy images of Raw 264.7 cells treated with SH-GQDs (200 μg/ml) at the excitation wavelength of 405 nm after incubation for 0.5 and 24 h (Scale bars = 50 μm).

that the oxLDL efflux rates in the presence of SH-GQDs increased in a time-dependent manner (Fig. 3a and b). Thus, the enhancement of lipid efflux from lipid-laden macrophages caused by SH-GQDs could be explored to prevent foam cell formation and subsequent atherosclerotic plaque progression.

Effects of SH-GQDs on the Amount of Nitric oxide (NO) Released

As NO is involved with the contractility and vascular remodeling, NO at the specific concentrations could be utilized as a potential therapeutic regulator. However, the protective efficacy of NO decreases, as the amount of NO produced from the macrophage activation process exceeds the maximal effective concentration. The cellular amount of NO produced in Raw264.7 upon being triggered by SH-GQDs or lipopolysaccharide (LPS) (i.e., a pro-inflammatory marker) was examined to determine whether or not they produce the extra NO.

The macrophages were incubated with varying concentrations of SH-GQDs, IL-4 or LPS, and the amount of NO in the supernatant culture medium is quantified using Griess colorimetric assay. It was found that a significantly greater amount of NO (21.1 ± 1.3 μM) was produced, when cells were treated with LPS (100 ng/ml) (Fig. 4a). However, the treatment of IL-4, an alternative macrophage activator, or SH-GQDs at the concentrations up to 0.1 mg/ml caused no difference in the amount of NO. In addition, SH-GQDs did not exert any inflammatory activities in the macrophages.

Effects of VEGF on the Amount of Nitric oxide (NO) Produced from hUVECs

Nitric oxide (NO) has been identified to play a crucial role in maintaining vasodilator tone of endothelium (22,28,29). In addition to vasodilation, platelet adhesion and leukocyte activation can be inhibited by NO (30).

The amount of NO released from hUVECs mediated by vascular endothelial growth factor (VEGF) was determined using Griess assay (31) after incubation of cells for 24 or 48 h (Fig. 4b). It was found that the amount of NO produced in the presence of VEGF (i.e., the positive control) significantly depends on exposure duration (0.4 ± 0.1 μM for 24 h; 1.7 ± 0.7 μM for 48 h). The amount of NO produced was substantially reduced, as hUVECs were treated with nitric oxide synthase (NOS) inhibitor, L-NAME (L-NAME: For 24 h, 0.13 ± 0.13 μM; 48 h, 0.8 ± 0.3 μM). When cells were treated with both VEGF and NOS, the amount of NO significantly increased, whereas hUVECs treated with oxLDL displayed no difference in the production of NO (oxLDL: 0.43 ± 0.13 μM for 24 h; 0.7 ± 0.4 μM for 48 h). The cells incubated concurrently with oxLDL and SH-GQDs significantly enhanced the amount of NO, which was similar to that from the positive control (1.87 ± 0.31 μM for 48 h exposure to 10 μg/ml of SH-GQDs).

It was previously demonstrated that SH-GQDs targeting lipid-laden macrophage reduced foam cell formation through down-regulating MSR expression and enhancing efflux of oxLDL (15). The integrated approach based on SH-GQDs could not only protect endothelium against oxLDL-mediated stress, but also facilitate to recover NO production from hUVECs. Subsequently, SH-GQDs can be utilized as a

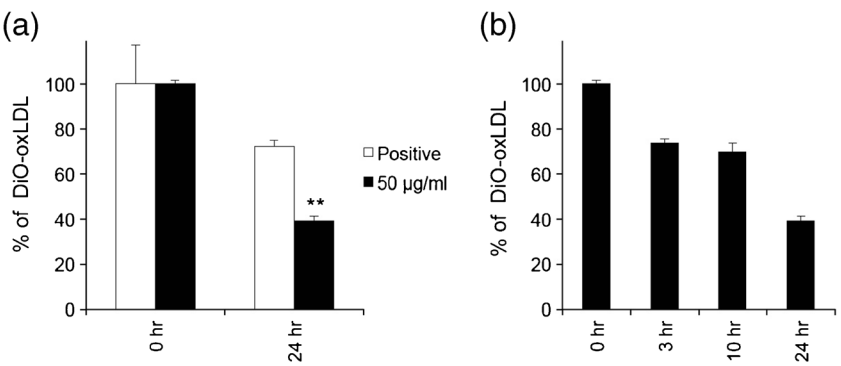

Fig. 3 (**a**) Efflux of oxLDL from Raw264.7 cells after pretreatment with DiO-oxLDL (2 μg/ml) was investigated using a flow cytometry. Raw264.7 cells were treated with two different groups: media control (positive) and SH-GQDs (50 μg/ml) (** indicates statistically significant difference between positive and SH-GQDs, $n = 3$, $p < 0.01$). (**b**) oxLDL efflux mediated by SH-GQDs treatment occurred in a time dependent manner ($n = 3$).

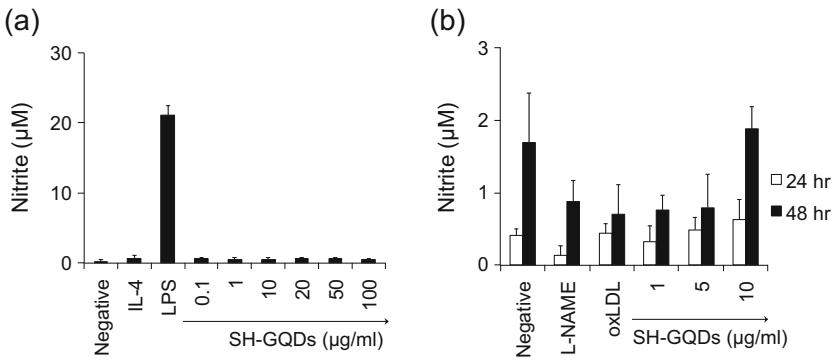

Fig. 4 (**a**) Assessment of nitric oxide (NO) release from Raw264.7 cells using Griess assay ($n = 5$). (**b**) Assessment of nitric oxide (NO) release from hUVECs using Griess assay ($n = 5$).

theranostic nano-carrier, guaranteeing high accessibility and visualization of nanomedicine to an atherosclerotic plaque, and simultaneously monitoring the progression of plaque.

Effects of SH-GQDs on Barrier Functions of hUVECs Against oxLDL

Impaired vaso-relaxation induced by oxLDL enhanced the risk of plaque progression and coronary artery disease (32,33). To monitor barrier function (i.e., permeability) of endothelial layer induced by oxLDL, the trans-endothelial electrical resistance (TEER) across the endothelial layer seeded on transwell plate was evaluated at various time intervals (1, 3, 6, 10 and 24 h). As shown in Fig. 5, hUVECs cultured on transwell inserts produced a well-defined endothelial monolayer with functional TEER (100 Ω-cm^2).

When media with oxLDL (10 μg/ml) were added into the insert wells, the barrier function of adherence junctions was significantly disrupted (oxLDL: 67.2 ± 2.2 Ω-cm^2 for 24 h). SH-GQDs (10 μg/ml) recovered impaired TEER to the initial status (SH-GQDs: 114.6 ± 8.5 Ω-cm^2 for 24 h), indicating that adherence junctions were preserved by SH-GQDs during the incubation process. However, GQDs significantly impaired TEER (GQDs: 67.9 ± 8.1 Ω-cm^2 for 24 h $p < 0.01$, $n = 3$), indicating that GQDs don't have an endothelium protective property against oxLDL. The maintenance of electrical permeability by SH-GQDs could lead to translocation of lipids across the permeable endothelium (i.e., the enhancement of lipid efflux) that can mitigate the plaque progression.

Scavenging Effects of SH-GQDs on Zebrafish Larvae

Although still in its infancy, there have been reports on distinctive advantages of zebrafish in elucidating the toxicity mechanism and identifying endpoints of toxicity. As shown in Fig. 6a, the embryonic periods (2 and 48 h-post fertilization (hpf)) were selected to visualize the embryo toxicity caused by SH-GQDs with two loading concentrations (0.1 and 1 mg/ml). An exposure of embryos to SH-GQDs (1 mg/ml) enhanced mortality, whereas a low dose (0.1 mg/ml) did not exert any harmful effects on embryos. The results indicated that the high concentration of SH-GQDs (1 mg/ml) exerted the embryo toxicity at early embryonic period (2 hpf), causing the disruption of fertilized embryos and subsequently leading to embryo death.

To investigate the amount of ROS accumulation in zebrafish larvae against H_2O_2, larvae were stained with ROS-sensitive dye (DCFDA). As shown in Fig. 6b, SH-GQDs-treated larvae displayed low fluorescence intensity as compared with the control, indicating that SH-GQDs have a protective role against oxidative stress. As the concentration of SH-GQDs increased, the fluorescence intensities decreased toward that of the negative control. These results demonstrated that the enhanced ROS levels caused by oxidative stress (i.e. H_2O_2) were significantly lowered by SH-GQDs. In addition, the high concentration of SH-GQDs caused the disruption of fertilized embryos, leading to embryo death.

Potential Toxicity of SH-GQDs on Zebrafish Embryos

Developmental toxicity on zebrafish embryos upon being treated with nanomaterials including silica nanoparticles and advanced nanoparticles have been extensively studied (17,34,35). It was previously reported that even though several zebrafish endpoints did not directly correlate to acute toxicity data conducted in rats or rabbits, zebrafish has shown its potential to be explored to examine acute toxicity of exogenous compounds and drug carriers (36). Because the heart

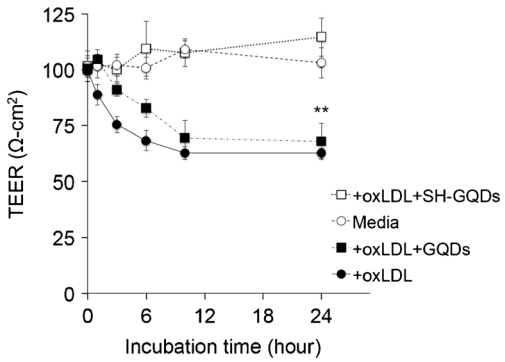

Fig. 5 Variation of TEER values in response to oxLDL, oxLDL + GQDs and oxLDL + SH-GQDs on Raw264.7 cells (** indicates statistically significant difference between groups, $n = 3$, $p < 0.01$).

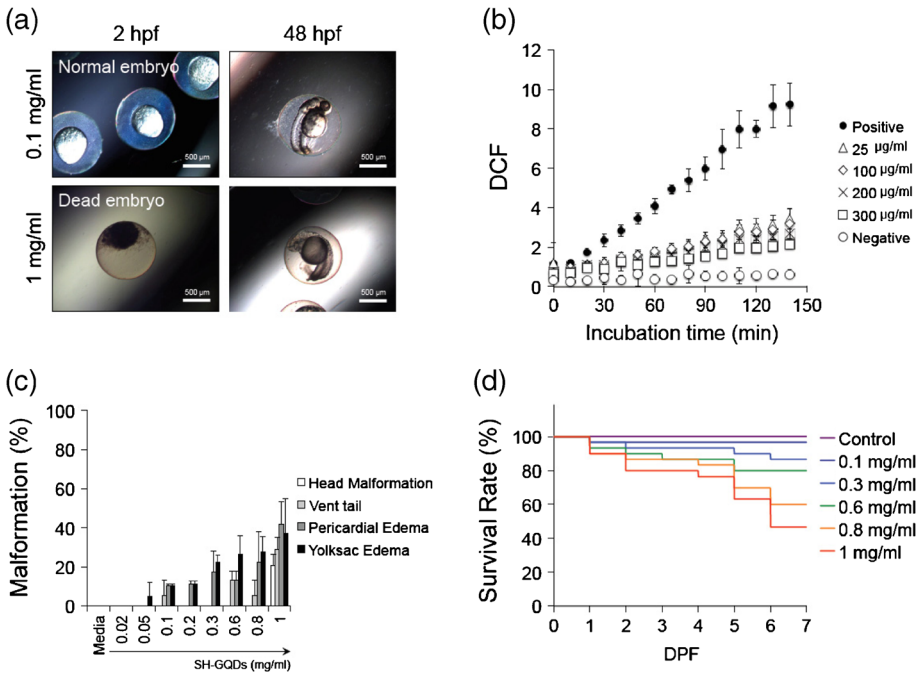

Fig. 6 (**a**) Photographs of zebrafish embryos exposed to SH-GQDs (0.1 and 1 mg/ml). (**b**) Quantitative measurements of DCF fluorescence using multimode detector (Ex: 485 nm; Em: 515 nm). Embryos were treated with H_2O_2 (50 μM) in presence of varying concentration of SH-GQDs (0, 25, 100, 200 and 300 μg/ml) ($n = 3$). (**c**) Malformation of zebrafish embryos exposed to SH-GQDs ($n = 20$). (**d**) Survival analysis of varying concentrations of SH-GQDs ($n = 30$).

development is a first step during the development process of embryos, zebrafish embryos has been used as a predictive model for toxicity studies on heart development (17,18,37,38).

To assess the *in vivo* toxicity of SH-GQDs on the cardiovascular system, various types of malformation at segmentation, hatching and fully developed larvae were examined. An exposure of zebrafish embryos to SH-GQDs resulted in malformations, such as head deformation, vent tail, pericardial edema and yolksac edema (Fig. 6c). The pericardial edema and yolk sac edema were found in zebrafish embryos treated with 0.1 mg/ml or greater concentrations of SH-GQDs. In addition, such abnormal configurations as head malformation, vent tail, pericardial edema and yolksac edema occurred, when zebrafish embryos were exposed to more than 0.8 mg/ml SH-GQDs.

It was previously reported that silica nanoparticles (100 μg/ml or higher) caused serious yolk sac and pericardial edema (17). Therefore, it was concluded that varying nano-sized materials, such as graphene quantum dots and silica nanoparticles, exerted malformation to some degrees depending on their concentration ranges, which should be thoroughly monitored.

Effects of SH-GQDs on the Survival Rate of Zebrafish Larvae

The survival rate of zebrafish larvae upon exposure to SH-GQDs was considered as a hallmark of identifying a potential toxicity. When they were incubated for the first day of days-post fertilization (dpf) with up to 1 mg/ml of SH-GQDs, at least 90% embryos from all the groups including the control group were still alive. The treatments with up to 1 mg/ml SH-GQDs did not affect the hatching success rate, either. However, the significantly higher mortality rates (46% for 1 mg/ml) were observed from the groups exposed to the higher concentrations of SH-GQDs at 7 dpf, indicating that the mortality rates were dependent on dose and exposure time of SH-GQDs. Therefore, the doses of SH-GQDs should be low enough to avoid any toxicity in their clinical applications. The results from the zebrafish model studies provide new insights into drug discovery, carrier toxicity and pathological diseases assessed from recent advances in genetic analysis coupled with high-throughput screening techniques.

CONCLUSION

SH-GQDs significantly enhanced the efflux of oxLDL and down-regulated macrophage scavenger receptor (MSR) in mouse macrophage cell line (Raw264.7). The ROS levels stimulated by oxidative stress (i.e. H_2O_2) were lowered by SH-GQDs. The relationship among the expression of macrophage scavenger receptor A (MSR-A), lipid accumulation and ROS production in macrophages was established to optimize SH-GQDs as an efficient preventive means against atherosclerosis. The studies with the zebrafish models indicated that the mortality rates of the zebrafish are dependent on dose and exposure time of SH-GQDs, and highlight the understanding of negligible side effects of SH-GQDs at the lower concentrations (~0.2 mg/ml). These studies further guarantee that SH-GQDs can serve as a nontoxic fluorescent probe for scientific and clinical usage against cardiovascular diseases.

REFERENCES

1. Stirrat CG, Newby DE, Robson JMJ, Jansen MA. The Use of Superparamagnetic Iron Oxide Nanoparticles to Assess Cardiac Inflammation | SpringerLink. Curr Cardiovasc Imaging Rep. 2014;7:9263.
2. Li M, Anastassiades CP, Joshi B, Komarck CM, Piraka C, Elmunzer BJ, et al. Affinity peptide for targeted detection of dysplasia in Barrett's esophagus. Gastroenterology. 2010;139(5):1472–80.
3. Atwal JK, Chen Y, Chiu C, Mortensen DL, Meilandt WJ, Liu Y, et al. A therapeutic antibody targeting BACE1 inhibits amyloid-beta production *in vivo*. Sci Transl Med. 2011;3(84):84ra43.
4. Seo JW, Baek H, Mahakian LM, Kusunose J, Hamzah J, Ruoslahti E, et al. (64)Cu-labeled LyP-1-dendrimer for PET-CT imaging of atherosclerotic plaque. Bioconjug Chem. 2014;25(2):231–9.
5. Stendahl JC, Sinusas AJ. Nanoparticles for Cardiovascular Imaging and Therapeutic Delivery, Part 1: Compositions and Features. J Nucl Med. 2015;56(10):1469–75.
6. Mustapha A, Hussain A, Samad SA, Zulkifley MA, Diyana Wan Zaki WM, Hamid HA. Design and development of a content-based medical image retrieval system for spine vertebrae irregularity. Biomed Eng Online. 2015;14:6.
7. Hofmann M, Steinke F, Scheel V, Charpiat G, Farquhar J, Aschoff P, et al. MRI-based attenuation correction for PET/MRI: a novel approach combining pattern recognition and atlas registration. J Nucl Med. 2008;49(11):1875–83.
8. Ding H, Wu F. Image Guided Biodistribution of Drugs and Drug Delivery. Theranostics. 2012;2(11):1037–9.
9. Perez-Medina C, Abdel-Atti D, Tang J, Zhao Y, Fayad ZA, Lewis JS, et al. Nanoreporter PET predicts the efficacy of anti-cancer nanotherapy. Nat Commun. 2016;7:11838.
10. Valeur B, Berberan-Santos MN. Molecular fluorescence: principles and applications, 2nd Ed.; 2012.
11. Jares-Erijman EA, Jovin TM. FRET imaging. Nat Biotechnol. 2003;21(11):1387–95.
12. Kelly K, Alencar H, Funovics M, Mahmood U, Weissleder R. Detection of invasive colon cancer using a novel, targeted, library-derived fluorescent peptide. Cancer Res. 2004;64(17):6247–51.
13. Lane LA, Smith AM, Lian T, Nie S. Compact and blinking-suppressed quantum dots for single-particle tracking in live cells. J Phys Chem B. 2014;118(49):14140–7.
14. Ma W, Xu W, Xu H, Chen Y, He Z, Ma M. Nitric oxide modulates cadmium influx during cadmium-induced programmed cell death in tobacco BY-2 cells. Planta. 2010;232(2):325–35.
15. Oh B, Lee CH. Development of Thiolated-Graphene Quantum Dots for Regulation of ROS in macrophages. Pharm Res. 2016;33(11):2736–47.
16. Kzhyshkowska J, Neyen C, Gordon S. Role of macrophage scavenger receptors in atherosclerosis. Immunobiology. 2012;217(5):492–502.
17. Duan J, Yu Y, Li Y, Sun Z. Cardiovascular toxicity evaluation of silica nanoparticles in endothelial cells and zebrafish model. Biomaterials. 2013;34(23):5853–62.
18. Bakkers J. Zebrafish as a model to study cardiac development and human cardiac disease. Cardiovasc Res. 2011;91(2):279–88.
19. Lieschke GJ, Trede NS. Fish immunology. Curr Biol. 2009;19(16):R678–82.
20. Renshaw SA, Trede NS. A model 450 million years in the making: zebrafish and vertebrate immunity. Dis Model Mech. 2012;5(1):38–47.
21. Zheng W, Li Z, Nguyen AT, Li C, Emelyanov A, Gong Z. Xmrk, Kras and Myc transgenic zebrafish liver cancer models share molecular signatures with subsets of human hepatocellular carcinoma. PLoS One. 2014;9(3).
22. Oh B, Lee CH. Advanced cardiovascular stent coated with nanofiber. Mol Pharm. 2013;10(12):4432–42.
23. Parker MO, Millington ME, Combe FJ, Brennan CH. Housing conditions differentially affect physiological and behavioural stress responses of zebrafish, as well as the response to anxiolytics. PLoS One. 2012;7(4):e34992.
24. Shang W, Zhang X, Zhang M, Fan Z, Sun Y, Han M, et al. The uptake mechanism and biocompatibility of graphene quantum dots with human neural stem cells. Nano. 2014;6(11):5799–806.
25. Petersen LK, York AW, Lewis DR, Ahuja S, Uhrich KE, Prud'homme RK, et al. Amphiphilic nanoparticles repress macrophage atherogenesis: novel core/shell designs for scavenger receptor targeting and down-regulation. Mol Pharm. 2014;11(8):2815–24.
26. Lewis DR, Petersen LK, York AW, Zablocki KR, Joseph LB, Kholodovych V, et al. Sugar-based amphiphilic nanoparticles arrest atherosclerosis *in vivo*. Proc Natl Acad Sci U S A. 2015;112(9):2693–8.
27. Li AC, Glass CK. The macrophage foam cell as a target for therapeutic intervention. Nat Med. 2002;8(11):1235–42.
28. Sandoo A, van Zanten JJV, Metsios GS, Carroll D, Kitas GD. The Endothelium and Its Role in Regulating Vascular Tone. Open Cardiovasc Med J. 2010;4:302–12.
29. Oh B, Lee CH. Nanofiber-coated drug eluting stent for the stabilization of mast cells. Pharm Res. 2014;31(9):2463–78.
30. McHugh J, Cheek DJ. Nitric oxide and regulation of vascular tone: pharmacological and physiological considerations. Am J Crit Care. 1998;7(2):131–40. quiz 141-132
31. Bussolati B, Dunk C, Grohman M, Kontos CD, Mason J, Ahmed A. Vascular endothelial growth factor receptor-1 modulates vascular endothelial growth factor-mediated angiogenesis via nitric oxide. Am J Pathol. 2001;159(3):993–1008.
32. Byfield FJ, Tikku S, Rothblat GH, Gooch KJ, Levitan I. OxLDL increases endothelial stiffness, force generation, and network formation. J Lipid Res. 2006;47(4):715–23.
33. Valente AJ, Irimpen AM, Siebenlist U, Chandrasekar B. OxLDL induces endothelial dysfunction and death via TRAF3IP2: inhibition by HDL3 and AMPK activators. Free Radic Biol Med. 2014;70:117–28.
34. Zhu X, Zhu L, Li Y, Duan Z, Chen W, Alvarez PJ. Developmental toxicity in zebrafish (*Danio rerio*) embryos after exposure to manufactured nanomaterials: buckminsterfullerene aggregates (nC60) and fullerol. Environ Toxicol Chem. 2007;26(5):976–9.
35. Wang K, Ma J, He M, Gao G, Xu H, Sang J, et al. Toxicity assessments of near-infrared upconversion luminescent LaF3:Yb, Er in early development of zebrafish embryos. Theranostics. 2013;3(4):258–66.
36. Ducharme NA, Reif DM, Gustafsson JA, Bondesson M. Comparison of toxicity values across zebrafish early life stages and mammalian studies: Implications for chemical testing. Reprod Toxicol. 2015;55:3–10.
37. Duan J, Yu Y, Shi H, Tian L, Guo C, Huang P, Zhou X, Peng S, Sun Z. Toxic effects of silica nanoparticles on zebrafish embryos and larvae. PLoS One. 2013;8(9).
38. Lin S, Zhao Y, Nel AE. Zebrafish: an *in vivo* model for nano EHS studies. Small. 2013;9:1608–18.